Monitoring root-zone soil moisture through the assimilation of a thermal remote sensing-based soil moisture proxy into a water balance model

Wade T. Crow and William P. Kustas

USDA ARS, Hydrology and Remote Sensing Laboratory, Beltsville, MD

John H. Prueger

USDA ARS, National Soil Tilth Laboratory, Ames, IA

Abstract

Two types of Soil Vegetation Atmosphere Transfer (SVAT) modeling approaches can be applied to monitor root-zone soil moisture in agricultural landscapes. Water and Energy Balance (WEB) SVAT modeling is based on forcing a prognostic root-zone water balance model with observed rainfall and predicted evapotranspiration. In contrast, thermal Remote Sensing (RS) observations of surface radiometric temperature (T_R) are integrated into purely diagnostic RS-SVAT models to predict the onset of vegetation water stress. While RS-SVAT models do not explicitly monitor soil moisture, they can be used in the calculation of thermal-based proxy variables for the availability of soil water in the root zone. Using four growing seasons (2001 to 2004) of profile soil moisture, micro-meteorology, and surface radiometric temperature measurements at the United States Department of Agriculture (USDA) Opti-

mizing Production Inputs for Economic and Environmental Enhancements (OPE^3) study site in Beltsville, MD, prospects for improving WEB-SVAT root-zone soil water predictions via the assimilation of diagnostic RS-SVAT soil moisture proxy information are examined. Results illustrate the potential advantages of such an assimilation approach relative to the competing approach of directly assimilating T_R measurements. Since T_R measurements used in the analysis are tower-based (and not obtained from a remote platform), a sensitivity analysis demonstrates the potential impact of remote sensing limitations on the value of the RS-SVAT proxy. Overall, results support a potential role for RS-SVAT modeling strategies in improving WEB-SVAT model characterization of root-zone soil moisture.

Key words: Thermal remote sensing, soil moisture, data assimilation, and surface radiometric temperature.

---

1 Introduction

The development of modeling techniques to estimate soil moisture availability beyond the near-surface has been an area of extensive research during the past decade. Currently, the most advanced approaches are based on the assimilation of remote sensing observations into soil-vegetation-atmosphere transfer (SVAT) models. Following Crow et al. (2005a), these models can be conceptually divided into thermal remote sensing (RS) and water and energy balance (WEB) approaches.

In RS-SVAT approaches, T_R is derived from thermal remote sensing on cloud-free days and combined with vegetation information obtained at visible and near-infrared wavelengths in order to solve the surface energy balance. By accurately interpreting thermal signals from vegetation, these approaches can

detect the increase in surface temperature - due to a reduction in evapotranspiration - occurring in canopies at the onset of water stress. Detection of these stress signals typically requires accurate ancillary vegetation cover information to distinguish between stressed vegetation and warm soil/substrate backgrounds (see e.g. Moran, 2003). RS-SVAT approaches are generally diagnostic in nature and make instantaneous predictions only for times at which remote surface T_R retrievals are available.

In contrast, WEB-SVAT approaches typically neglect T_R observations and make energy flux predictions by parameterizing components of the surface energy balance as a function of surface aerodynamic temperature and numerically solving the balance equation to predict surface energy fluxes. These flux predictions are then combined with rainfall observations and vertical modeling of the soil column in order to continually track soil moisture. Soil water stress is diagnosed when predicted root-zone soil moisture falls below a predefined level and triggers an increase in vegetation stomatal resistance. If available, T_R observations can be used to constrain WEB-SVAT predictions through data assimilation. A number of past studies have developed techniques to directly assimilate T_R observations into WEB-SVAT models with the goal of improving surface energy flux and profile soil moisture estimates (van den Hurk et al., 1997; Jones et al., 1998; Lakshmi, 2000; Bosilovich et al. 2006). Additional work has also focused on the assimilation of surface (0-5 cm) soil moisture retrievals obtained from microwave remote sensing (Houser et al., 1998; Walker et al., 1999; Margulis et al., 2002; Reichle et al., 2005).

As a result of their structural differences, RS- and WEB-SVAT models use fundamentally different approaches to predict surface energy fluxes and diagnose the availability of root-zone soil moisture. Crow et al. (2005a) demon-

strate that, even when forced with consistent meteorological and vegetation information, the structural differences between WEB- and RS-SVAT modeling approaches are profound enough that errors in surface energy flux estimates produced by both models are statistically independent. Such independence can be exploited using data assimilation or integration approaches designed to filter errors in continuous WEB-SVAT state predictions based on the consideration of instantaneous RS-SVAT retrievals. A small number of past studies have exploited this potential by inserting RS-SVAT evapotranspiration predictions directly into a water balance model (Meijerik et al., 2005), using RS-SVAT energy flux predictions to constrain WEB-SVAT model parameter selection (Franks and Beven, 1999), or employing simple data assimilation techniques to update WEB-SVAT soil moisture predictions using RS-SVAT evapotranspiration predictions (Schuurmans et al., 2003).

Despite these advances, little is currently known about the potential for improving WEB-SVAT soil moisture estimates via the assimilation of RS-SVAT retrievals. As noted above, the direct assimilation of T_R observations offers an alternative approach for the integration of thermal remote sensing observations into a WEB-SVAT model. Therefore, a key unresolved issue is whether any rationale exists for processing T_R observations through a RS-SVAT model prior to their assimilation. Here we use a four-year soil moisture and T_R data set within an agricultural site to evaluate the accuracy of a RS-SVAT-based root-zone soil moisture proxy and the potential for improving root-zone soil moisture predictions through the assimilation of this proxy into a WEB-SVAT model. Assimilation results are compared to the competing approach of directly assimilating T_R observations. The modeling and Ensemble Kalman filter (EnKF) data assimilation strategy used in the analysis will be presented in

Section 2. Modeling and data assimilation results are discussed in Section 3, and Section 4 describes a sensitivity analysis aimed at quantifying the impact of limitations in satellite-based T_R retrievals on results.

2 Approach

Both RS- and WEB-SVAT modeling strategies are based on the partitioning of net radiation (R_N) into sensible heating (H), latent heating (LE), and ground heat flux (G) components via solution of separate surface energy balance equations for the vegetation canopy (C) and soil surface (S)

$$R_{N,C} = H_C + LE_C \tag{1}$$
$$R_{N,S} = H_S + LE_S + G_S. \tag{2}$$

Observations of downward solar ($S_\downarrow$) and longwave radiation ($L_\downarrow$) at the top of the vegetation canopy are decomposed into incident canopy and soil radiation components based on the radiative transfer model of Campbell and Norman (1998). These components are then used to calculated $R_{N,C}$ and $R_{N,S}$ as

$$R_{N,C} = (1 - \tau_{\text{longwave}})(L_\downarrow + \epsilon_S \sigma T_S^4 - 2\epsilon_C \sigma T_C^4) + (1 - \tau_{\text{solar}})(1 - \alpha_C) S_\downarrow \tag{3}$$
$$R_{N,S} = \tau_{\text{longwave}} L_\downarrow + (1 - \tau_{\text{longwave}})\epsilon_C \sigma T_C^4 - \epsilon_S \sigma T_S^4 + \tau_{\text{longwave}}(1 - \alpha_S) S_\downarrow \tag{4}$$

where ϵ, τ, and α refer to emissivity, canopy transmissivity and albedo parameters, respectively, and σ is the Stephen-Boltzman constant. Total surface flux quantities are obtaining by summing canopy and surface components (e.g. $LE = LE_C + LE_S$). Subsequent differences in RS- and WEB-SVAT modeling approaches are described below.

The RS-SVAT modeling approach employed here is based on the parallel version of the two-source model (TSM) methodology originally described in Norman et al. (1995). The TSM parameterizes sensible heating from the vegetation canopy and soil surface as

$$H_C = \rho C_p \frac{T_C - T_A}{R_A} \tag{5}$$

$$H_S = \rho C_p \frac{T_S - T_A}{R_A + R_{A,S}} \tag{6}$$

where ρ is the density of air, C_p the specific heat of air, R_A the above canopy aerodynamic resistance term, $R_{A,S}$ the within canopy aerodynamic resistance, T_A the air temperature, T_S the soil temperature, and T_C the canopy temperature. The parameterization of R_A and $R_{A,S}$ is based on assumed surface roughness lengths, wind speed, and stability considerations presented for the parallel version of the TSM in Norman et al. (1995). A more complicated series resistance formulation was also developed by Norman et al. (1995) allowing more complete interaction between soil and canopy components. However, differences in flux predictions from the parallel and series formulations are minor in most cases (Norman et al., 1995; Li et al., 2005). Neglecting emissivity differences between the canopy and the soil (Kustas and Norman, 1997), T_S and T_C can be constrained by the observed surface radiometric temperature (T_R) and

$$T_R = [f_{\text{veg}} T_C^4 + (1 - f_{\text{veg}}) T_S^4]^{1/4} \tag{7}$$

where f_{veg} is the areal fraction of the sensor field of view occupied by vegetation predicted as a function of leaf area index (LAI) and look angle (θ) as

$$f_{\text{veg}} = 1 - \exp\left(\frac{-\text{LAI}}{2\cos(\theta)}\right). \tag{8}$$

Ground heat flux in (2) is modeled as

$$G_S = c_g R_{N,S} \tag{9}$$

where the variation of c_g according to LAI and time of day follows the algorithm presented in Kustas et al. (1998).

As a first guess, the TSM estimates LE_C according to the Priestly-Taylor formula

$$LE_C = f_g \alpha_{PT} \frac{s}{s+\gamma} R_{N,C} \tag{10}$$

where α_{PT} is the Priestley-Taylor constant (typically taken to be $\sim$1.3 for unstressed vegetation), s is the first-derivative of the Clauius-Claperon equation with respect to temperature, and f_g is the "green" fraction of the canopy actively transpiring. Using this estimate of LE_C, and independent knowledge of $R_{N,C}$, (1) is solved for H_C and (5) inverted to estimate T_C as

$$T_C = (1 - f_g \alpha_{PT} \frac{s}{s+\gamma}) R_{N,C} \frac{R_A}{\rho C_p} + T_A. \tag{11}$$

The constraint in (7) can then be inverted to estimate T_S as

$$T_S = \left(\frac{T_R^4 - f_{\text{veg}} T_C^4}{1 - f_{\text{veg}}}\right)^{1/4}. \tag{12}$$

Prediction of T_S allows for calculation of H_S via (6) and consequently LE_S as the residual of (2)

$$LE_S = (1 - c_g)R_{N,S} - \rho C_p \frac{T_S - T_A}{R_A + R_{A,S}}. \tag{13}$$

If the vegetation canopy is under soil moisture stress, assuming $\alpha_{PT} = \sim 1.3$ in (10) will overestimate LE_C and lead to the underestimation of T_C in (11) and the overestimation of T_S in (12). Since it is calculated as a residual in (13), such temperature biases will eventually manifest themselves as a negative bias in LE_S. In normal application of the TSM this problem is addressed by iteratively lowering α_{PT} in (10) to ensure LE_S predictions are greater than zero (Kustas and Norman, 1999). However, if this iterative correction is not employed, uncorrected LE_S values will reflect both the direct impact of near-surface water limitations on soil evaporation as well as the impact of propagating biases arising from the overestimation of LE_C via (10). Consequently, water limitations in both the surface- and root-zone will both act to reduce uncorrected LE_S predictions obtained from (13). Based on this reasoning, we define a soil moisture proxy S_{TSM} equal to the value of LE_S obtained from (13) when α_{PT} is held equal to ~ 1.3.

Following the approach of Reichle and Koster (2005), TSM-based S_{TSM} retrievals are rescaled prior to assimilation into a WEB-SVAT model such that their temporal mean (μ) and standard deviation (σ) matches that of WEB-SVAT root-zone soil moisture predictions (θ_{rz})

$$\theta_{\mathrm{rz}}^{\mathrm{TSM}} = \mu_{\theta_{\mathrm{rz}}} + (S_{\mathrm{TSM}} - \mu_{S_{\mathrm{TSM}}}) \frac{\sigma_{\theta_{\mathrm{rz}}}}{\sigma_{S_{\mathrm{TSM}}}}. \tag{14}$$

The skill of $\theta_{\rm rz}^{\rm TSM}$ in capturing vertically integrated root-zone soil water dynamics will be empirically determined through comparisons with profile soil moisture measurements in Section 3.

2.2 WEB-SVAT modeling

The WEB-SVAT modeling employed here was derived from merging the force-restore model introduced by Noilhan and Planton (1989), and adapted by Montaldo and Albertson (2001), with a two-layer vegetation/soil energy balance formulation utilizing a vertical canopy structure identical to that employed by the parallel version of the TSM (Norman et al., 1995). The force-restore water balance model conceptually divides the soil column into two reservoirs: a surface zone and a root-zone. These two zones are overlapping such that the surface zone constitutes the top fraction of the root zone. The balance equation for the surface zone soil moisture ($\theta_{\rm sz}$) is

$$\frac{d\theta_{\rm sz}}{dt} = \frac{C_1}{d_{\rm sz}}[P_g - LE_S(\rho_w\lambda)^{-1}] - \frac{C_2}{\tau_d}(\theta_{\rm sz} - \theta_{\rm eq}) \tag{15}$$

where P_g is precipitation through-fall, τ_d the frequency of diurnal variations (24 hours), ρ_w the density of water, λ the latent heat of vaporization for water, and $d_{\rm sz}$ the depth of the surface zone. Variables C_1 and C_2 are soil texture and soil moisture dependent quantities and $\theta_{\rm eq}$ is a function of root-zone soil moisture ($\theta_{\rm rz}$) such that the second term in (15) estimates the diffusive flux of water between the surface and bulk root zone (Noilhan and Planton, 1989; Montaldo et al., 2001). For the root zone, the analogous balance equation is

$$\frac{d\theta_{\rm rz}}{dt} = \frac{1}{d_{\rm rz}}[P_g - LE_C(\rho_w\lambda)^{-1} - LE_S(\rho_w\lambda)^{-1} - Q] \tag{16}$$

where LE_C is plant canopy transpiration, d_{rz} the root-zone soil depth, and Q drainage out the bottom of the root zone parameterized using soil saturated hydraulic conductivity K_s, porosity θ_{sat}, and the pore size distribution index parameter b as

$$Q = Ks\left(\frac{\theta_{\mathrm{rz}}}{\theta_{\mathrm{sat}}}\right)^{2b+3}. \tag{17}$$

Precipitation is partitioned into canopy storage and P_g by updating canopy storage (θ_c) following

$$\frac{d\theta_c}{dt} = P - E_{\mathrm{WC}} \tag{18}$$

where E_{WC} is direct (or "wet") canopy evaporation and P is observed rainfall incident on the canopy. The vegetation canopy is assumed to posses a maximum water holding capacity of LAI/5 [mm]. When θ_c is below this threshold, P_g equals zero, and when θ_c exceeds this threshold, $P_g = P$. Runoff is produced when either (15) or (16) estimates a soil moisture value that exceeds θ_{sat}.

For consistency with the TSM: G_S is modeled as a fraction of $R_{N,C}$ following (9), $R_{N,C}$ and $R_{N,S}$ are modeled following (3) and (4), and H_C and H_S are based on (5) and (6). However, in contrast to the TSM, WEB-SVAT LE_C and LE_S predictions are based on

$$LE_S = [e_s(T_S) - e_a]\rho_w C_P \gamma^{-1}/(R_{A,S} + R_A + R_S) \tag{19}$$
$$LE_C = [e_s(T_C) - e_a]\rho_w C_P \gamma^{-1}/(R_C + R_A) \tag{20}$$

where e_s is the saturation vapor pressure and e_a the above canopy vapor pressure. The direct canopy evaporation E_{WC} is estimated by setting $R_C = 0$ in (20) and dividing by $\rho_w C_P$ to obtain volume flux units. Following Sellers et al.

(1992) the soil resistance to vapor flux R_S (in units of m s^{-1}) is parameterized as an empirical function of $\theta_{\rm sz}$

$$R_S = \exp[A - B(\theta_{\rm sz}/\theta_{\rm sat})]. \tag{21}$$

The stomatal resistance to transpiration R_C is estimated using the typical simple piecewise relationship with root-zone soil moisture

$$R_C = \begin{cases} R_{C,\max} & \theta_{\rm rz} < \theta_w \\ (R_{C,\min} - R_{C,\max})\frac{\theta_{\rm rz}-\theta_w}{\theta^*-\theta_w} + R_{C,\max} & \theta_w < \theta_{\rm rz} < \theta^* \\ R_{C,\min} & \theta_{\rm rz} > \theta^*. \end{cases} \tag{22}$$

The volumetric soil moistures at which canopy stress θ^* and wilting θ_w begins are calculated using soil hydraulic parameters and assuming matrix potentials of -2.1 and -100 Mb for the onset of stress and wilting, respectively. Resistance extremes $R_{C,\max}$ and $R_{C,\min}$ are specified based on typical literature values.

The overall computational stream for the WEB-SVAT model is as follows. Water-balance estimates of $\theta_{\rm sz}$ and $\theta_{\rm rz}$ are used to calculate the resistance variables in (21) and (22) which, in turn, allow all flux terms in (1) and (2) to be expressed in terms of T_C and T_S. The simultaneous solution of (1) and (2) for T_C and T_S - via a numerical root finder - provides the soil evaporation (LE_S) and canopy transpiration (LE_C) estimates required to update water state variables and step forward in time via (15), (16) and (18). Given knowledge of $f_{\rm veg}$, WEB-SVAT predicted surface radiometric temperature can then be obtained from (7).

The study domain is the Optimizing Production Inputs for Economic and Environmental Enhancements (OPE^3) site located at the USDA-ARS Beltsville Area Research Center in Beltsville, Maryland during the 2001 to 2004 growing seasons. Local soil texture is characterized as several meters of sandy loam sand overlying an impermeable clay lens. The topographic structure of the clay lens has been demonstrated to exert strong control over patterns of lateral subsurface flow within the site (Gish et al., 2005). Land cover is cultivated corn typically planted in May or June and harvested in October or November.

Micro-meteorological and eddy covariance instrumentation are mounted on a 10-m tower at the OPE^3 site to measure $L_{\downarrow}$, $S_{\downarrow}$, T_R, LE, H, G_S and meteorological observations. Sampling frequency is 10 Hz for the eddy covariance and 0.1 Hz for the energy balance and meteorological instrumentation. Air temperature (T_a) and e_a are measured using Vaisala HMP 45C sensors mounted at 4 and 8 m agl, P using Texas Instruments TE-525 gauges at 2.5 and 6 m agl, and T_R using an Apogee Inc. IRTS-P3 infrared radiative thermometer mounted at 4.5 m. Incoming and outgoing radiation are measured with a Kipp and Zonen, Inc. CNR-1 radiometer at 4.5 m above ground level (agl) [Trade and company names are given for the benefit of the reader and imply no endorsement by USDA]. Net radiation is also measured with a Kipp and Zonen NR-Lite at 2.5 m agl and a Radiation Energy Balance Systems, Inc. Q*7 net radiometer also at 2.5 m agl. A Campbell Scientific, Inc. 3-D sonic anemometer and a LI-COR LI7500 infrared hygrometer positioned at 4 m agl are used to measure H and LE flux densities as the covariance of the vertical wind velocity with air temperature and water vapor density. Friction velocity

and vertical velocity statistics are computed from the sonic anemometer. For G_S, six REBS soil heat flow transducers (HFT-1) are buried 0.08 m below the soil surface. Above each soil heat flux plate at 0.02 and 0.06 m depth are two Type-T soil thermocouples. The soil temperature data are used to compute the storage component of G above the flux plates. Soil moisture measurements are based on EnviroSCAN capacitance probe sensors installed at five separate sites within 50 meters of the flux tower. A weighted average of probe measurements available at depths of 10, 30, 50, and 80 cm is used to obtain a vertically integrated, top 1-meter representation of root-zone soil moisture.

The eddy covariance data were processed with temperature and relative humidity measurements used to correct for oxygen and density effects on the evaporative and CO_2 fluxes (Webb-Pearman-Leuning-WPL correction; Webb et al., 1980). Further processing included applying a 2-D coordinate transformation (coordinate rotation-CR) forcing horizontal components of wind speed to zero (Kaimal and Finnigan, 1994). As is the case with most study sites employing the eddy covariance technique, there is a general lack of energy balance closure among the flux measurements, which are caused by any number of site and instrumental factors (Foken et al., 2006). Following the suggestion of Li et al. (2005), closure in the flux measurements was enforced by adding the residual balance term (i.e. $R_n - LE - H - G$) to LE observations.

Figure 1 shows time series of observed T_R, LAI, root-zone soil moisture (θ_{rz}), and daily eddy correlation-based evapotranspiration ($E_T = LE\ (\rho_w \lambda)^{-1}$) measurements for the site during the 2001, 2002, 2003 and 2004 growing seasons. The 2002 growing season was unusually dry and exhibits clearly defined stress signals in θ_{rz} and E_T observations (Figure 1). In contrast, 2003 was wetter than normal - especially during early portions of the growing seasons. 2001

and 2004 were roughly typical with regards to growing season rainfall. The solid line in the LAI graphs (second row) represents the assumed piece-wise linear model for LAI temporal dynamics. The extensive LAI measurements needed to fully parameterize this fit are available only in 2004. For 2001 to 2003, the dynamics observed during the 2004 growing season were integrated with available information concerning crop emergence dates (vertical dashed lines in LAI plots) and mature-canopy LAI measurements near the IRT in order estimate the LAI time series.

2.4 Model parameterization and evaluation

Plant-canopy height h was assumed to follow the same piecewise-linear model as LAI except vertically rescaled to have a minimum of 0.1 m and a maximum of 2 m. Roughness lengths for momentum and heat transfer were assumed equal to $h/8$, and zero plane displacement height was set to $2h/3$. Canopy greenness (f_g) fraction was parameterized as remaining at unity until canopy LAI reached a maximum and then slowly declining at a rate of 0.005 day^{-1}. All soil parameters were set equal to sandy loam lookup table values presented in Cosby et al. (1984) and Noilhan and Planton (1989). The top layer of the WEB-SVAT model was given a depth of 5 cm and the second layer a depth of 1 m. Stomatal resistance values $R_{C,\min}$ and $R_{C,\max}$ were set equal to 100 and 5000 s m^{-1}. Following Kustas et al. (1998), the unitless parameters A and B in (21) were set equal to 8.2 and 4.3, respectively. At the start of the growing season, soil moisture variables in the WEB-SVAT models are assumed to match observed levels at the OPE^3 site. Due to changes in the frequency of archived and quality-controlled micro-meteorological observations, the WEB-

SVAT model was run on a 10-minute time step in 2001 and 2002, and a 30-minute time step for 2003 and 2004.

The comparison of baseline WEB-SVAT predictions with OPE^3 data resulted in several small changes to the model. The original WEB-SVAT model initially over-predicted T_R and under-predicted $\theta_{\rm sz}$ during the early portions of the growing season (not shown). This was corrected by setting C_1 in (15) to unity - thus neglecting the more complicated treatment discussed in Noilhan and Planton (1989) - and forcing $R_{A,S}$ to zero for short (i.e. $h < 25$ cm) vegetation canopies. In addition, $\theta_{\rm rz}$ was better predicted during later portions of the growing season by using a calibrated value of 3.0 for b and not the default value of 4.34 suggested by Cosby et al. (1984) for a sandy loam soil. Given the rather ad hoc nature of these changes, their influence on key results will be discussed later in the paper.

After the changes outlined above, WEB-SVAT and RS-SVAT/TSM predictions results were compared to ground-based observations available at the OPE^3 site. Comparisons between WEB-SVAT and TSM E_T predictions and eddy-correlation observations in Figure 2 suggest a slightly superior performance for the TSM with regards to surface energy fluxes. However, it should be noted that the small positive bias seen in TSM E_T predictions would increase if energy flux observations are closed via conservation of the Bowen ratio (H/LE) and not by adding the residual energy balance term to LE. In addition, with the exception of a high bias in early season T_R for 2003, WEB-SVAT predictions of $\theta_{\rm rz}$ (Figure 3) and T_R (Figure 4) are generally quite good. Extremely low T_R observations during the early portion of the 2003 growing season suggest the presence of standing water. The WEB-SVAT model is unable to capture either the overall wetness of this period (see Figure 3) or the

potential impact of standing water on T_R (Figure 4).

2.5 Data assimilation approach

Data assimilation is based on the use of an Ensemble Kalman filter (EnKF) to sequentially assimilate either $\theta_{\mathrm{rz}}^{\mathrm{TSM}}$ retrievals or T_R observations into the WEB-SVAT model. A sequential approach is adopted to reflect our expectation that the approach will eventually be used for real-time monitoring of root-zone soil water availability, The EnKF was been widely applied to land data assimilation applications in recent years and it generally considered a least as accurate on competing sequential filters (e.g. Reichle et al., 2002). Its approach is based on generating an ensemble of model realizations, each perturbed in a Monte Carlo manner, to obtain the forecast error covariance information required by the standard Kalman filter update equation. To create the ensemble, a mean-zero Gaussian perturbation term δ is added to WEB-SVAT θ_{rz} state predictions obtained via (16). Generated perturbations are statistically independent both in time and across the forecast ensemble. At times in which RS-SVAT $\theta_{\mathrm{rz}}^{\mathrm{TSM}}$ retrievals are available, θ_{sz} and θ_{rz} state variables associated with the ith Monte Carlo model replicate are collected in the state vector $\mathbf{\Theta}^i$. Given the availability of a $\theta_{\mathrm{rz}}^{\mathrm{TSM}}$ observation, this vector is updated via

$$\mathbf{\Theta}^{i+} = \mathbf{\Theta}^{i-} + \mathbf{K}(\theta_{\mathrm{rz}}^{\mathrm{TSM}} + v^i - \theta_{\mathrm{rz}}^{i-}) \tag{23}$$

where v is a noise term sampled independently for each model replicate from a mean-zero Gaussian distribution with variance (C_v) equal to the uncertainty of the rescaled $\theta_{\mathrm{rz}}^{\mathrm{TSM}}$ observation. Plus (+) and minus (-) superscript notation

indicates quantities before and after updating. The Kalman filter gain $\mathbf{K}$ is given by

$$\mathbf{K} = [\mathbf{C_{YM}}(C_M + C_v)^{-1}]. \tag{24}$$

where C_M is the (scalar) variance of the WEB-SVAT θ^i_{rz} forecasts ($\theta^{i-}_{\mathrm{rz}}$) and $\mathbf{C_{YM}}$ is a vector containing the variance of $\theta^{i-}_{\mathrm{rz}}$ and the covariance between $\theta^{i-}_{\mathrm{rz}}$ and $\theta^{i-}_{\mathrm{sz}}$. Both quantities are obtained by statistically sampling $\theta^{i-}_{\mathrm{rz}}$ and $\theta^{i-}_{\mathrm{sz}}$ and replicates around their ensemble means.

After updating via (23), ensemble components of the updated state vector $\mathbf{\Theta}^{i+}$ are propagated in time following (15) and (16) - and further perturbed by additive δ noise - until the next $\theta^{\mathrm{TSM}}_{\mathrm{rz}}$ observation becomes available and the updating procedure is repeated. Final WEB-SVAT/EnKF state predictions are obtained by averaging $\mathbf{\Theta}^i$ replicates across the entire ensemble.

In addition to the assimilation of $\theta^{\mathrm{TSM}}_{\mathrm{rz}}$, this analysis will consider the competing methodology of directly assimilating T_R observations. For this case, the update equation in (23) is modified to

$$\mathbf{\Theta}^{i+} = \mathbf{\Theta}^{i-} + \mathbf{K}(T_R + v^i - T^{i-}_{R,\mathrm{WEB}}) \tag{25}$$

where $T^{i-}_{R,\mathrm{WEB}}$ is the WEB-SVAT T_R prediction for the ith model replicate. No rescaling is applied to T_R measurements prior to their assimilation. The Kalman gain $\mathbf{K}$ in (25) is also slightly modified so that C_M and C_v represent scalar variances of $T_{R,\mathrm{WEB}}$ and T_R observations, respectively, and $\mathbf{C_{YM}}$ is a vector containing the covariance between $T^{i-}_{R,\mathrm{WEB}}$ and both $\theta^{i-}_{\mathrm{rz}}$ and $\theta^{i-}_{\mathrm{sz}}$. As before, $\mathbf{C_{YM}}$ and C_M are obtained by sampling Monte Carlo replicates around the ensemble mean.

A critical aspect of any EnKF application is specifying the variance of δ (C_δ - used to perturb model forecasts and represent WEB-SVAT forecast uncertainty) and v perturbations (C_v - used to represent either T_R or $\theta_{\rm rz}^{\rm TSM}$ observational uncertainty) terms. Filter innovations

$$\nu =< \theta_{\rm rz}^{\rm TSM} - \theta_{\rm rz}^{i-} > \text{ or } \nu =< T_R - T_{R,\rm WEB}^{i-} >, \tag{26}$$

where brackets indicate averaging across the ensemble, provide a valuable diagnostic tool for constraining these values. If all the assumptions underlying the optimality of the EnKF filter are met and errors are perfectly represented in a statistical sense, then the resulting times series of ν should be mean zero and have a variance of $C_M + C_v$. Given an independent estimate of C_v, the C_δ variance term can be tuned until this theoretical constraint is met (Dee, 1995). Satisfying this constraint implies that the model ensemble is correctly representing actual forecast uncertainties.

3 Results

Soil moisture information derived from the TSM is expressed in terms of the $\theta_{\rm rz}^{\rm TSM}$ proxy value obtained at 14 Local Solar Time (LST) (19 GMT). Figure 3 shows the time series of TSM $\theta_{\rm rz}^{\rm TSM}$ retrievals during the 2001 to 2004 growing seasons. Gaps in $\theta_{\rm rz}^{\rm TSM}$ retrievals reflect days where solar radiative forcing is deemed too low ($S_\downarrow < 600$ W m^{-2}) for surface stress signals to clearly register in T_R observations. Figure 5 demonstrates the relationship between all $\theta_{\rm rz}^{\rm TSM}$ retrievals and root-zone (0-1 meter averaged) soil moisture observations. Despite lumping retrievals obtained over a wide range of both inter- and intra-annual surface variability (see Figure 1), the scatterplot reveals a single, relatively

well-defined relationship between $\theta_{\rm rz}^{\rm TSM}$ retrievals and observed $\theta_{\rm rz}$. The offset from a one-to-one line observed in the scatterplot is due to a differences in the dynamic range of the WEB-SVAT model (whose climatology $\theta_{\rm rz}^{\rm TSM}$ has been scaled into) and observed root-zone soil moisture.

3.1 Assimilation of $\theta_{\rm rz}^{\rm TSM}$ into WEB-SVAT

Using (14) and statistics calculated from long-term (2001 to 2004) TSM and WEB-SVAT simulations at the OPE^3 site, 14 LST (19 GMT) $S_{\rm TSM}$ retrievals are rescaled into a $\theta_{\rm rz}^{\rm TSM}$ time series whose temporal mean and variance matches that of the WEB-SVAT model $\theta_{\rm rz}$ predictions. The observation error variance C_v is calculated by linearly rescaling observed root-zone (0-1 meter) soil moisture values plotted along the x-axis of Figure 5 into the WEB-SVAT model's climatology - using an approach analogous to (14) - and then calculating a mean-squared difference with $\theta_{\rm rz}^{\rm TSM}$. During the EnKF assimilation analysis, a 30-member Monte Carlo ensemble of WEB-SVAT $\mathbf{\Theta}^i$ predictions is obtained by specifying C_δ and perturbing WEB-SVAT $\theta_{\rm rz}$ predictions obtained via (16). Members of this ensemble are updated via (23) using $\theta_{\rm rz}^{\rm TSM}$ retrievals obtained from the TSM model. Because of presumably lower soil moisture skill in $\theta_{\rm rz}^{\rm TSM}$ retrievals during cloudy days, only 14 LST (19 GMT) $\theta_{\rm rz}^{\rm TSM}$ retrievals concurrent with downward solar forcing ($S_\downarrow$) greater than 600 W m^{-2} are assimilated. This corresponds to about 65% of days during the 2001-2004 growing seasons. The entire EnKF procedure is repeated for various choices of C_δ until the time series of filter innovations ν is mean zero with variance $C_M + C_v$. Once the filter is properly tuned, WEB-SVAT/EnKF results are obtained by averaging state predictions across the ensemble.

Figures 6 demonstrates Case WEB-SVAT/EnKF data assimilation results for a period of the 2002 growing season. Case 1 (see Table 1) results reflect modeling results obtained using: calibrated soil hydraulic parameters, start-of-season initialization using soil moisture observations, and precipitation data obtained from a well-maintained, on-site rain gauge. Consequently, errors in Case 1 WEB-SVAT predictions reflect only the impact of structural shortcomings in the WEB-SVAT modeling approach. For example, its inability to capture the lateral movement of root-zone water known to occur at the site (Gish et al., 2005). WEB-SVAT modeling predictions shown in Figures 2, 3, and 4 reflect Case 1 results. In contrast, Case 2 (see Table 1) is based on the degradation of Case 1 by using: default soil hydraulic parameters, a default spring soil moisture initial condition (i.e. $\theta_{\rm rz} = 0.20$ cm^{3}cm^{-3}), and hourly rainfall observations for the site derived from continental-scale North American Land Data Assimilation (NLDAS) precipitation products (Cosgrove et al., 2003). Consequently, Case 2 reflects model parameterization and forcing difficulties typically encountered when applying WEB-SVAT models over larger spatial domains.

Figure 7 displays scatterplots of modeled versus observed root-zone soil moisture for both modeling cases - with and without the EnKF-based assimilation of TSM/RS-SVAT $\theta_{\rm rz}^{\rm TSM}$ retrievals. For WEB-SVAT modeling Case 1 (top row), relatively little improvement is observed when assimilating $\theta_{\rm rz}^{\rm TSM}$. In contrast, clear improvement in the correlation between WEB-SVAT modeled and observed $\theta_{\rm rz}$ is found for assimilation into Case 2 WEB-SVAT modeling results. Accounting for the reduction in the degrees of freedom within WEB-SVAT predictions due to serial auto-correlation (Van Storch and Zwiers, 1999), the increase in correlation for assimilation into Case 2 is significant at a 93%

confidence level.

The need to rescale TSM soil moisture proxy observations into the WEB-SVAT model climatology presents a potential obstacle to the real-time operation of a sequential filter since multi-year climatological statistics are required to rescale S_{TSM} observations via (14) before assimilation analysis can be initiated. To examine the impact of poorly-sampled climatological statistics derived from shorter time periods, assimilation results in Figure 7 were re-run using climatological statistics derived from sampling only a single growing season (instead of all four between 2001 and 2004). These results (not shown) demonstrated only minor sensitivity to such a reduction. Depending on the single year chosen, correlation coefficient results (R^2) for the assimilation of $\theta_{\mathrm{rz}}^{\mathrm{TSM}}$ (Case 2) changed from 0.69 to between 0.63 and 0.70. Consequently, the need to acquire climatological statistics for rescaling does not appear to a be a significant barrier for the real-time functioning of the filter. However, the requirement to rescale observations into the WEB-SVAT model's climatology does preclude the assimilation of $\theta_{\mathrm{rz}}^{\mathrm{TSM}}$ from correcting existing bias and/or dynamic range problems in WEB-SVAT soil moisture predictions. As a result, the impact of assimilation on RMS error statistics remains small (Figure 7).

3.2 Assimilation of T_R into WEB-SVAT

An obvious alternative to the assimilation of $\theta_{\mathrm{rz}}^{\mathrm{TSM}}$ is the direct assimilation of T_R observations underlying TSM predictions. Figure 8 is equivalent to Figure 7 except it demonstrates results for the EnKF-base assimilation of T_R instead of $\theta_{\mathrm{rz}}^{\mathrm{TSM}}$. In contrast to $\theta_{\mathrm{rz}}^{\mathrm{TSM}}$ assimilation results, no marginal benefit is seen for either modeling case when T_R is directly assimilated. In addition, while

the removal of ad hoc changes made to improve WEB-SVAT T_R predictions (see Section 2.4) has little effect on $\theta_{\rm rz}^{\rm TSM}$ assimilation results in Figure 7, it will further degrade T_R assimilation results in Figure 8.

Difficulties encountered in directly assimilating T_R measurements can be traced to a number of potential sources. First, the relationship between $\theta_{\rm rz}$ and T_R predictions is dependent on a range of variables (e.g. wind speed, air temperature, surface roughness, vegetation coverage and surface albedo) other than $\theta_{\rm rz}$. Uncertainty in any of these factors can confound the accurately updating of $\theta_{\rm rz}$ using T_R observations. In addition - even if perfectly specified - the relationship between T_R and $\theta_{\rm rz}$ is highly nonlinear and not well suited for the application of Kalman filtering techniques. Figure 9 shows examples of the relationship for typical summertime afternoon micro-meteorology conditions (T_A = 20 C, relative humidity = 60%, S$\downarrow$ = 700 W m^{-2} and wind speed = 3 ms^{-1}) and a range of LAI magnitudes between 0.5 and 2.5. EnKF updating results in Figure 8 are based on (25) and a linear approximation to the relationship between WEB-SVAT $\theta_{\rm rz}$ predictions and T_R retrievals. The inability of (25) to capture the nonlinear nature of this relationship will introduce error and potential instabilities into WEB-SVAT/EnKF predictions. In apparent contrast to T_R, the relationship between $\theta_{\rm rz}$ and $\theta_{\rm rz}^{\rm TSM}$ is approximately linear and relatively well-defined even when expressed by lumping observations obtained over a wide range of micro-meteorological, soil moisture and vegetative conditions (Figure 5). As a result, processing T_R observations through the TSM/RS-SVAT modeling framework results in a functional relationship with $\theta_{\rm rz}$ that is more amenable to application of the EnKF.

4 Impact of remote sensing limitations

As discussed in Section 2, this analysis uses tower-based infrared thermometer data to estimate T_R. Consequently it neglects important accuracy and temporal sampling issues inherent in the retrieval of T_R from satellite platforms. For instance, a key limitation of spaceborne thermal sensors is the restriction of surface retrievals to sufficiently cloud-free days. This impact is examined in Figure 10 where the availability of T_R measurements is limited to days passing a variable minimum solar loading ($S_\downarrow$) threshold. Gradually increasing the $S_\downarrow$ threshold, used to define a "cloud-free" scene, naturally leads to a decrease in the frequency of 14 LST $\theta_{\rm rz}^{\rm TSM}$ retrievals (open squares in Figure 10a) available for assimilation. However, since the strongest coupling between thermal canopy observations and soil moisture occurs on days with the highest solar loading, increasing the required minimum $S_\downarrow$ threshold also increases the observed correlation between $\theta_{\rm rz}^{\rm TSM}$ and root-zone soil moisture observations (filled circles in Figure 10a). That is, utilizing a higher $S_\downarrow$ threshold is associated with acquiring lower frequency, but higher quality, soil moisture information. Because of this trade-off, the accuracy of Case 2 WEB-SVAT/EnKF $\theta_{\rm rz}$ results (obtained via the assimilation of $\theta_{\rm rz}^{\rm TSM}$) are relatively insensitive to the choice of a minimum $S_\downarrow$ threshold (Figure 10b). In fact, relatively good WEB-SVAT/EnKF results are obtained even when restricting the availability of $\theta_{\rm rz}^{\rm TSM}$ retrievals to only the 10% of days exhibiting the highest 14 LST $S_\downarrow$. As a result, the impact of temporal frequencies limitations inherent in the retrieval of T_R, and thus $\theta_{\rm rz}^{\rm TSM}$, from satellites is expected to be small.

For sun-synchronous, polar orbiting satellites, an additional concern is the appropriate time of day for T_R measurement acquisition. All results to this

point have been based on the specification of 14 LST for T_R acquisition. Figure 11 examines the sensitivity of Case 2 WEB-SVAT/EnKF $\theta_{\rm rz}$ (again acquired through the assimilation of $\theta_{\rm rz}^{\rm TSM}$) to this choice. Results demonstrated a window of relatively good performance between 11 and 14 LST with a slight peak at 13 LST. Consequently, results obtained at 14 LST appear roughly representative for any mid-day (11 to 14 LST) overpass time. $\theta_{\rm rz}^{\rm TSM}$ retrievals obtained from overpass times before or after this window will possess relatively less value as a root-zone soil moisture proxy.

In addition to temporal sampling limitations, satellite-based T_R observations will also suffer from accuracy limitations due to errors in the correction of atmospheric radiative transfer effects. In Figure 12 we capture the impact of such error by adding synthetic, temporally uncorrelated, Gaussian noise to tower-based T_R measurements. Increasing the magnitude of this noise clearly reduces the observed correlation between $\theta_{\rm rz}^{\rm TSM}$ retrievals and root-zone soil moisture observations (open squares in Figure 12). However, only modest sensitivity is observed for Case 2 WEB-SVAT/EnKF $\theta_{\rm rz}$ correlation results (solid circles in Figure 12). As the quality of T_R observations is degraded, the EnKF approach shifts weight away from $\theta_{\rm rz}^{\rm TSM}$ retrievals derived from T_R observations and onto WEB-SVAT predictions. A properly constructed filter should never degrade the accuracy of WEB-SVAT prediction below the open-loop modeling case of no data assimilation (dashed line in Figure 12). As a consequence, added value for WEB-SVAT modeling is noted even for relatively noisy T_R observations.

Finally, the strength of correlation between $\theta_{\rm rz}^{\rm TSM}$ retrievals and root-zone soil moisture observations in Figure 5 is partially dependent on the accuracy of vegetation input parameters (e.g. f_{veg}) inputted into the TSM. Here these

parameters are estimated based on observations of crop emergence dates and a single measurement of mature canopy LAI (see Figure 1 and Section 2); however, their estimation from remote sensing observations will likely entail greater uncertainty. The impact of this uncertainty can be captured through a sensitivity analysis based on the regeneration of Figure 5 in the presence of random, additive perturbations (with standard deviations of 0.5 and 7 days, respectively) to observed mature canopy LAI and yearly crop emergence dates. Results from this analysis demonstrate only minor sensitivity to such perturbations. The correlation coefficient (R^2) in Figure 7 (0.67) is reduced to an average of 0.65 in the case of perturbing mature canopy LAI and an average of 0.64 in the case of perturbing the yearly crop emergence date.

5 Discussion and Summary

At the USDA OPE^3 site, four-growing seasons worth of WEB-SVAT and RS-SVAT modeling results are obtained and compared with ground-based evapotranspiration (Figure 2), vertically integrated root-zone soil moisture (Figure 3), and surface radiometric temperature observations (Figure 4). RS-SVAT root-zone estimates are based on the definition of a new root-zone soil moisture proxy $\theta_{\mathrm{rz}}^{\mathrm{TSM}}$ which reflects the ability of the Two Source RS-SVAT model (TSM) to balance net radiation and match surface radiometric temperature observations given an assumption of unstressed canopy transpiration. Comparisons between this proxy and root-zone soil moisture observations demonstrate a significant level of linear correlation (Figure 5). This correlation can be exploited through the application of a Ensemble Kalman filtering (EnKF) data assimilation approach that integrates instantaneous $\theta_{\mathrm{rz}}^{\mathrm{TSM}}$ retrievals into con-

tinuous WEB-SVAT modeling (Figure 6). Assimilation results demonstrate the magnitude of improvement expected in two separate WEB-SVAT modeling scenarios when $\theta_{\mathrm{rz}}^{\mathrm{TSM}}$ retrievals are sequentially assimilated. Marginal improvement is noted for assimilation into a properly calibrated and forced models (Cases 1 in Figure 7). However, added value - significant at a 93% confidence level - is evident when the WEB-SVAT modeling approach is degraded with regards to its initialization, precipitation forcing and parameterization (Cases 2 in Figure 7). Overall, this suggests that the ultimate value of assimilating RS-SWAT soil moisture proxies may be to mitigate the degradation of WEB-SVAT modeling results associated with non-ideal model parameterization, initialization and forcing.

A key issue for this type of analysis is the relative advantage of assimilating $\theta_{\mathrm{rz}}^{\mathrm{TSM}}$ versus the direct assimilation of the T_R observations. Figure 8 addresses this issue by replicating Figure 7 for the case of directly assimilating T_R observations. However, in contrast to Figure 7, no added value for WEB-SVAT soil moisture predictions is associated with the assimilation of T_R. A key reason for this lack of success is the highly nonlinear relationship existing between T_R and θ_{rz} (Figure 9). The assimilation of $\theta_{\mathrm{rz}}^{\mathrm{TSM}}$ appears to circumvent this nonlinearity (see Figure 5) - suggesting that the processing of T_R observations through the RS-SVAT TSM prior to their assimilation may enhance the ultimate value of thermal remote sensing observations for data assimilation applications.

This analysis uses tower-based IRT observations instead of actual remote sensing data. Consequently it neglects temporal sampling and accuracy limitations that would be encountered when using actual remote sensing data. However, Figure 10 demonstrates that days associated with the best remote-sensing

based retrieval of T_R (i.e. cloud-free days with high solar loading) are also the same days in which $\theta_{\rm rz}^{\rm TSM}$ retrievals provide the greatest amount of information concerning root-zone soil moisture. That it, satellite-based $\theta_{\rm rz}^{\rm TSM}$ retrievals will tend to be available on the days in which they provide the most soil moisture information. Consequently, limitations in the frequency of satellite-based T_R observations due to cloud cover will not compromise the accuracy of assimilation results. Relatively modest sensitivity is also observed with respect to the time of day (Figure 11), the accuracy of T_R observations (Figure 12), and the specification of vegetation parameters (Section 4) - implying that the approach can be successfully scaled to satellite-based T_R observations.

Nevertheless, two important limitations must be considered when interpreting results. First, our particular choice of $\theta_{\rm rz}^{\rm TSM}$ as a soil moisture proxy is based on the empirical interpretation of results in Figure 5 and not a firm theoretical description of the relationship between $\theta_{\rm rz}^{\rm TSM}$ and $\theta_{\rm rz}$. Additional study will be required to validate the relationship seen in Figure 5 over a wider range of land surface and meteorological conditions. In addition, since $\theta_{\rm rz}^{\rm TSM}$ measurements are linearly re-scaled to match the WEB-SVAT model's climatology, $\theta_{\rm rz}^{\rm TSM}$ assimilation is incapable of correcting for the impact of model bias and/or an incorrect model dynamic range. However, it should be noted that - due to large model-to-model variability in the climatology of WEB-SVAT soil moisture predictions (Koster and Milly, 1997) - such rescaling is necessary for the assimilation of any remotely sensed soil moisture product (Drusch et al. 2004). Given this reality, the eventual benefit of any type of remotely-sensed soil moisture data for WEB-SVAT modeling is likely to be realized in the area of improved anomaly detection rather than bias or dynamic range correction (Crow et al., 2005b).

6 Acknowledgements

The authors would like to thank the logistical support in operating and maintaining the OPE^3 site as well as data collection and archiving efforts of Drs. Craig Daughtry, Timothy Gish and Greg McCarty of the USDA-ARS Hydrology and Remote Sensing Lab. The micrometeorological tower data were made available through the efforts of biological science technician Mr. Andy Russ of the Hydrology and Remote Sensing Laboratory.

References

Bosilovich, M.G., Radakovich, J.D., da Silva, A., Tolding, R., Frances, V. (2006). Skin temperature analysis and bias correction in a coupled land-atmosphere data assimilation system. *J. Met. Soc. Japan*, in press.

Drusch, M., Wood, E.F., and Gao, H. (2005). Observation operators for the direct assimilation of TRMM microwave imager retrieved soil moisture. *Geophys. Res. Letts.*, *32*, L15403, doi:10.1029/2005GL023623.

Campbell, G.S. and Norman, J.M. (1998). *An Introduction to Environmental Geophysics*. Springer-Verlag, New York, 286 pp.

Cosby, B.J., Hornberger, G.M., Clapp, R.B., and Ginn T.R. (1984). A statistical exploration of the relationships of soil moisture characteristics to the physical properties of soils. *Wat. Resour. Res.*, *20*, 682–690.

Cosgrove et al. (2003). Real-time and retrospective forcing in the North American Land Data Assimilation System (NLDAS) project. *J. Geophys. Res.*, *108*(D22), 8842, doi:10.1029/2002JD003118.

Crow, W.T., Li, F., and Kustas, W.P. (2005a). Intercomparison of spatially

explicit models for predicting surface energy flux patterns during the 2002 SMACEX field experiment. *J. Hydrometeorol.*, *6*, 941–953.

Crow, W.T., Koster, R., and Reichle, R. (2005b). Relevance of time-varying and time-invariant retrieval error sources on the utility of spaceborne soil moisture products. *Geophys. Res. Lett.*, *32*, L24405, doi:10.1029/2005GL024889.

Dee, D.P. (1995). On-line estimation of error covariance parameters for atmospheric data assimilation. *Mon. Wea. Rev.*, *123*, 1128–1145.

Franks, S.W., and Beven, K.J. (1999). Conditioning a multi-patch SVAT model using uncertain time-space estimates of latent heat fluxes as inferred from remotely-sensed data. *Water Resour. Res.*, *35*, 2751–2761.

Foken, T., Wimmer, F., Mauder, M., Thomas, C. and Liebethal, C. (2006). Some aspects of the energy balance closure problem. *Atmospheric Chemistry Physics Discussions*, *6*, 3381–3402.

Gish, T.J., Walthall, C.L., Daughtry, C.S.T., and Kung, K.-J. S. (2005). Using soil moisture and spatial yield patterns to identify subsurface flow pathways. *J. Environ. Qual.*, *34*, 274–286, 2005.

Houser, P.R., Shuttleworth, W.J., Famglietti, J.S, Gupta, H.V., Syed, K.H., and Goodrich, D.C. (1998). Integration of soil moisture remote sensing and hydrologic modeling using data assimilation. *Wat. Resour. Res.*, *34*, 3405–3420.

Jones, A.S., Guch I.C., and von der Haar, T.H. (1998). Data assimilation of satellite-derived heating rates as proxy soil wetness data into a regional atmospheric model. Part: I: Methodology. *Mon. Wea. Rev.*, *126*, 634–645.

Kaimal, J.C., and Finnigan, J.J. (1994). Atmospheric Boundary Layer Flows, Their Structure and Measurement, Oxford University Press, New York, 289 pp.

Koster R.D., and Milly, P.C. (1997). The interplay between transpiration and runoff formulations in land surface schemes used in atmospheric models. *J. Climate*, *10*, 1578–1591, 1997.

Kustas, W. P. and Norman, J. M. (1997). A two-source approach for estimating turbulent fluxes using multiple angle thermal infrared observations. *Wat. Resour. Res.*, *33*, 1495–1508.

Kustas, W.P., Zhan, X., and Schmugge, T.J. (1998). Combining optical and microwave remote sensing for mapping energy fluxes in a semiarid watershed. *Remote Sens. Environ.*, *64*, 116–131.

Kustas W.P., and Norman, J.M. (1999). Evaluation of soil and vegetation heat flux predictions using a simple two-source model with radiometric temperature for partial canopy cover. *Agric. For. Meteorol.*, *94*, 13–29.

Kustas, W.P., Anderson, M.C., Norman, J.M. and Li, F. (2006). Utility of Radiometric-Aerodynamic Temperature Relations for Heat Flux Estimation. *Boundary-Layer Meteorology.* (In Press)

Li, F., Kustas, W.P., Prueger, J.H., Neale, C.M.U., Jackson, T.J. (2005). Utility of Remote Sensing Based Two-Source Energy Balance Model Under Low and High Vegetation Cover Conditions. *Journal of Hydrometeorology*, *6*, 878–891.

Margulis, S.A., McLaughlin, D., Entekhabi, D., and Dunne, S. (2002). Land data assimilation of soil moisture using measurements from the Southern Great Plains 1997 Field Experiment. *Wat. Resour. Res.*, *38,* 1299, doi:10.1029/2001WR001114.

Lakshmi, V. (2000). A simple surface temperature assimilation scheme for use in land surface models. *Water Resour. Res.*, *36*, 3687–3700.

Meijerink, A.M.J., Gieske, A.S.M., and Vekerdy, D. (2005). Surface energy balance using satellite data for the water balance of a traditional irrigation-

wetland system in SW Iran, *Irrigration and Drainage Systems*, *19*, 89–105.

Montaldo, N., Albertson, J.D., Marcini, M., and Kiely, G. (2001). Robust prediction of root zone soil moisture from assimilation of surface soil moisture. *Water Resour.Res.*, *37*, 2889–2900.

Moran, M.S. (2003). Thermal responses as indicators of biophysical system health and integrity. In *Thermal Infrared Remote Sensing in Land Surface Properties*, Quattrochi, D.A., Luvall, J.C. (Eds.), CRC Press, Washington D.C., 257–282.

Noilhan, J.,and Planton, S. (1989). A simple parameterization of land surface processes in meteorologic models. *Mon. Weath. Rev.*, *117*, 536–549.

Norman, J.M., Kustas, W.P., and Humes, K.S. (1995). A two-source approach for estimating soil and vegetation energy fluxes in observations of directional radiometric surface temperature. *Agric. For. Meteorol.*, *77*, 263–293.

Reichle, R.H., Walker, J.P., Koster, R.D. and Houser, P.R. (2002). Extended vs. ensemble kalman filtering for land data assimilation. *J. Hydrometeorol.*, *3,* 728–740.

Reichle, R.H. and Koster, R.D. (2005). Global assimilation of satellite surface soil moisture retrievals into the NASA Catchment land surface model. *Geophys. Res. Lett.*, *32*, L02404, doi:10.1029/2004GL021700.

Sellers, P.J., Hesier, M.D., and Hall, F.G. (1992). Relations between surface conductance and spectral vegetation indices at intermediate (100 m^2 to 15 km^2) length scales. *J. Geophys. Res.*, *97*(D17), 19033–19059.

Schuurmans, J.M., Troch, P.A., Veldhuizen, A.A., Bastiaanssen, W.G.M. and Bierkens, M.F.P. (2003). Assimilation of remotely sensed latent heat flux in a distributed hydrological model. *Adv. Water. Resour.*, *26*, 151–159.

van den Hurk, B., Bastiaanssen, W., Pelgrum, H., and Meijgaard, E.V. (1997). A new methodology for assimilation of initial soil moisture fields in weather

prediction models using Meteosat and NOAA data. *J. Appl. Met.*, *37*, 1217–1233.

von Storch, H, and Zwiers, F.W. (2002). Statistical Analysis in Climate Research. Cambridge University Press, 494 pp.

Walker, J.P., Willgoose, G.R., and Kalma, J.D. (1999). One-dimensional soil moisture profile retrieval by assimilation of near-surface measurements: A simplified soil moisture model and field application. *J. Hydrol.*, *2*, 356–373.

Webb, E.K., Pearman, G.I., and Leuning, R. (1980). Correction of flux measurements for density effects due to heat and water vapor transfer. *Quar. Jour. Roy. Meteorol. Soc.*, *106*, 85–100.

Table 1

Description of WEB-SVAT modeling Cases 1 and 2.

	Case 1	Case 2
Initialization	Observed θ_{rz}	Default (θ_{rz}=0.20 $\mathrm{cm}^3\mathrm{cm}^{-3}$)
Parameters	Calibrated (b=2.8)	Default (b=4.3)
Precip. Source	Local Gauge	NLDAS

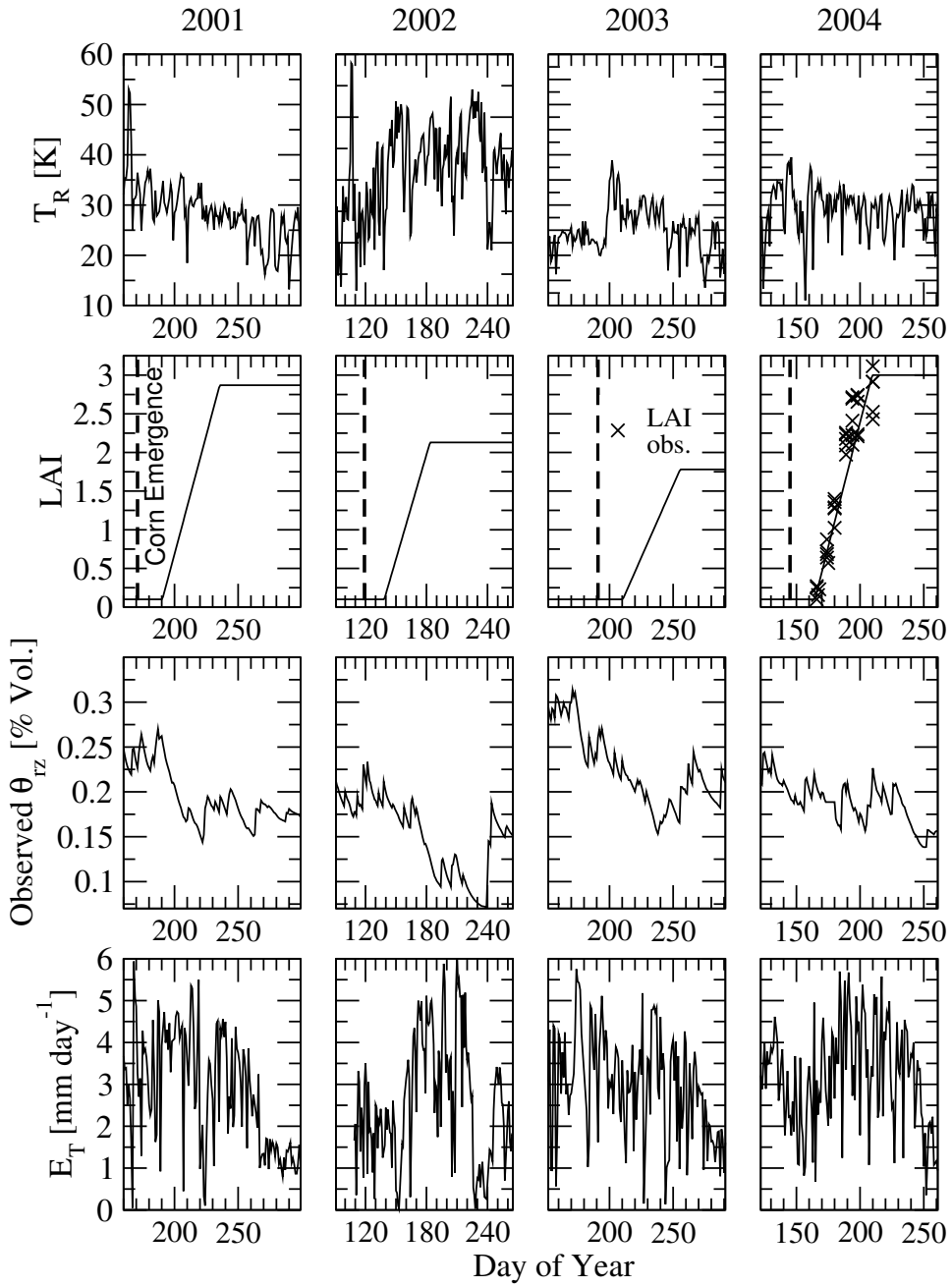

Fig. 1. Observed surface radiometric temperature (T_R), leaf area index LAI, root-zone soil moisture ($\theta_{\rm rz}$) and evapotranspiration (E_T) at the OPE^3 study site during the 2001, 2002, 2003 and 2004 growing seasons. Plotted T_R and $\theta_{\rm rz}$ values are based on 14 LST (19 GMT) observations. E_T observations are daily totals.

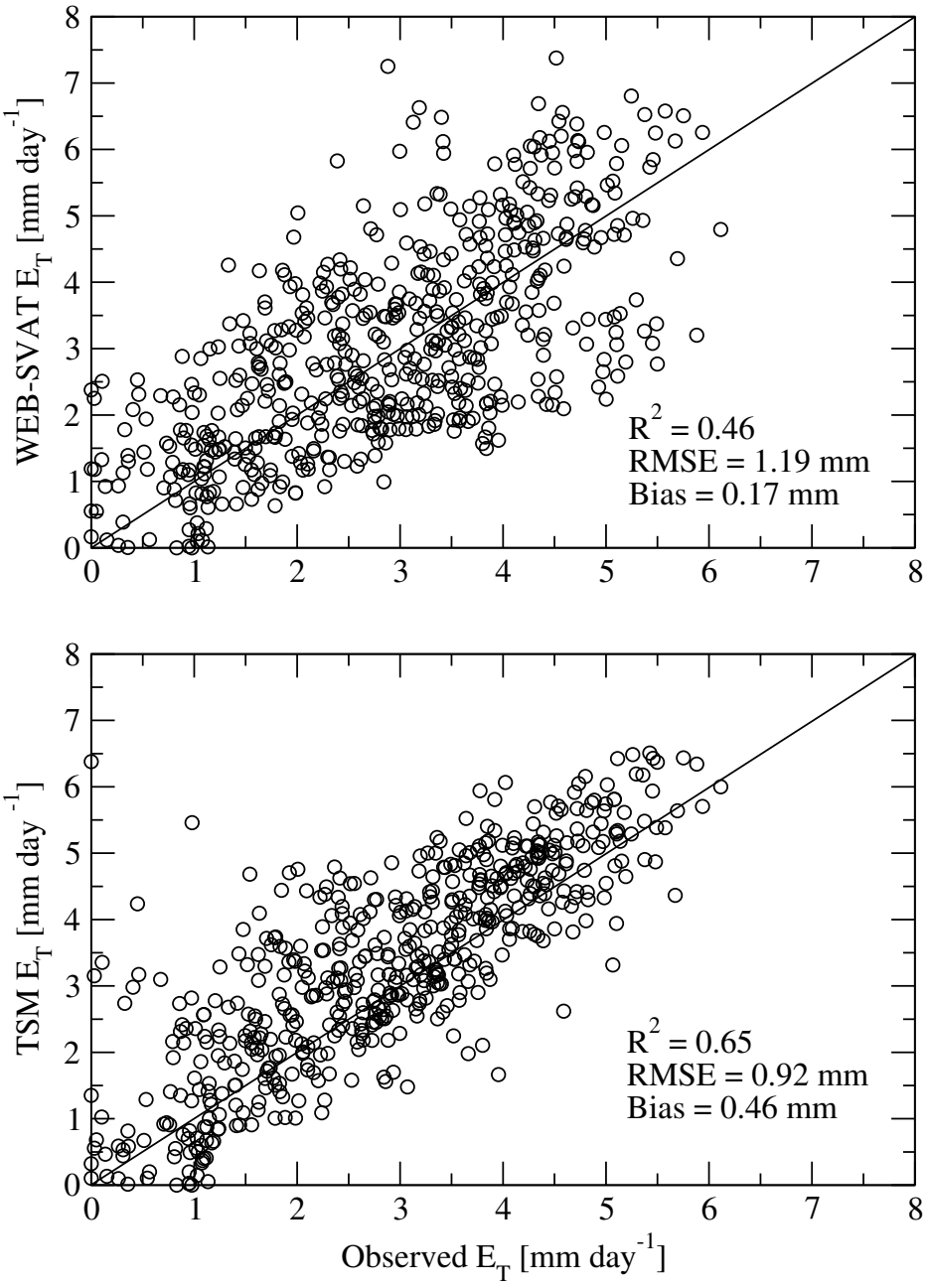

Fig. 2. Daily E_T predictions for both the TSM and WEB-SVAT models versus eddy correlation flux tower observations. Plotted points represent lumped daily data from the 2001, 2002, 2003 and 2004 growing seasons.

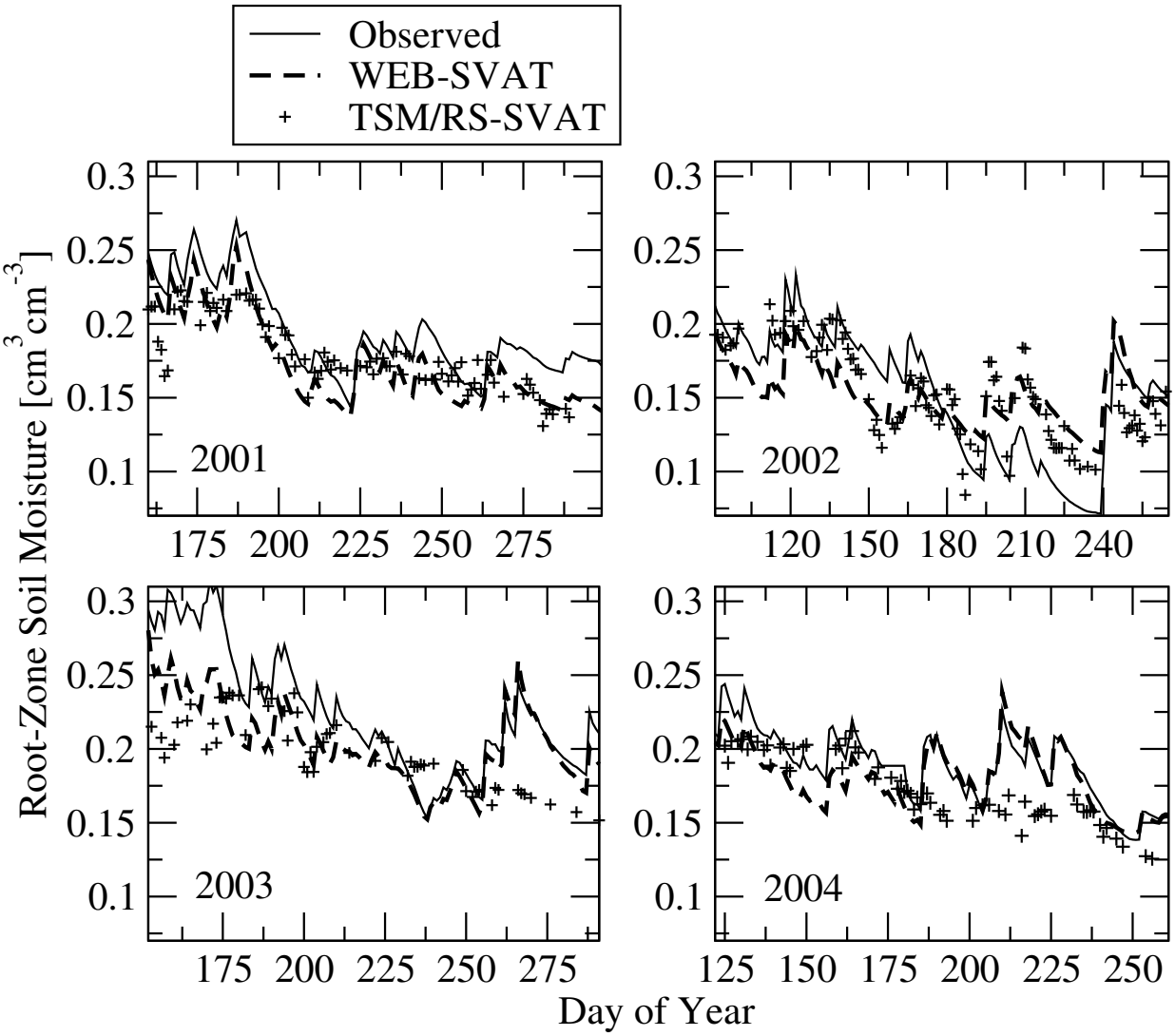

Fig. 3. Time series for observed root-zone soil moisture, WEB-SVAT root-zone soil moisture and the TSM/RS-SVAT soil moisture proxy ($\theta_{\rm rz}^{\rm TSM}$) during the 2001, 2002, 2003 and 2004 growing seasons.

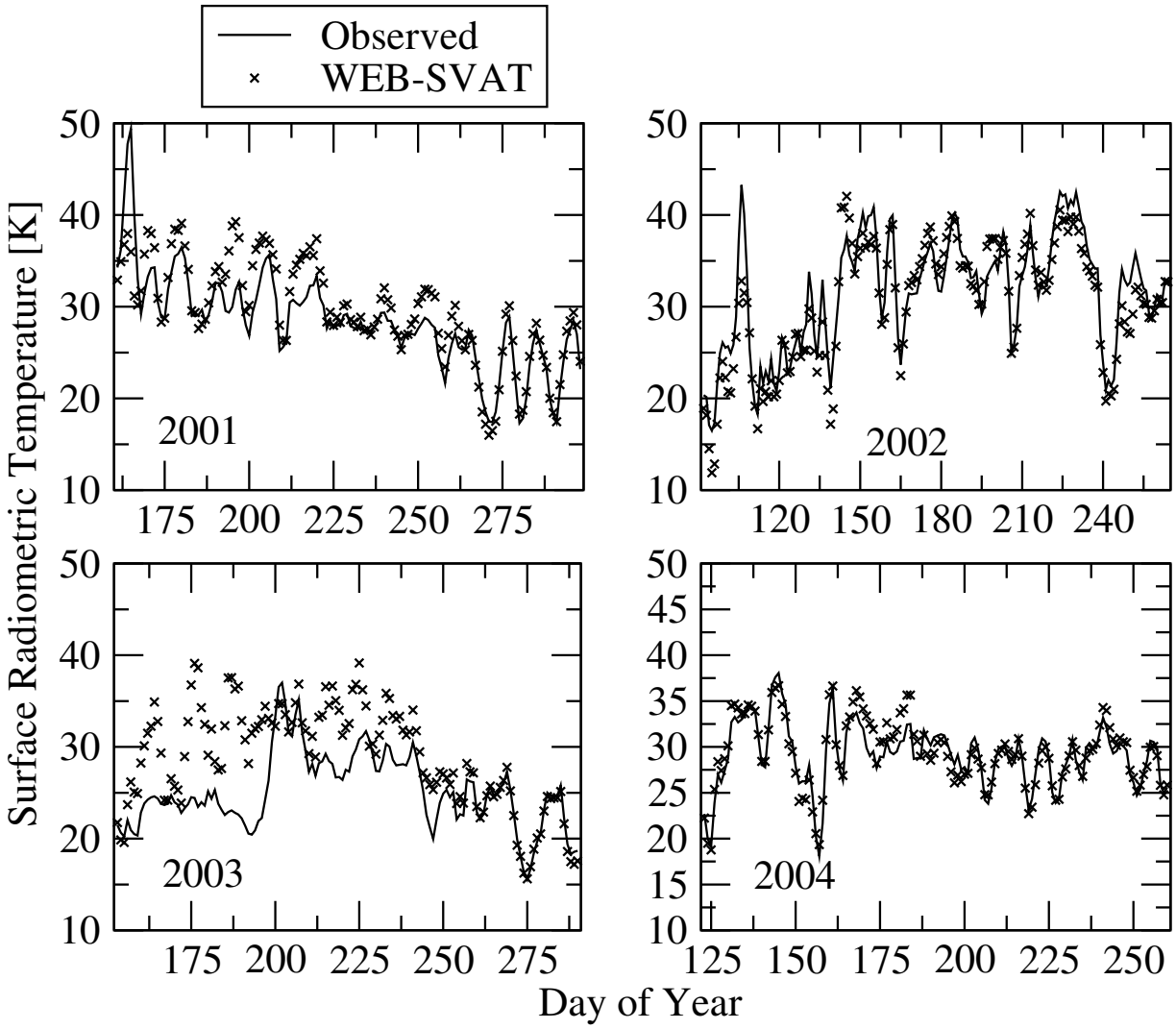

Fig. 4. Time series for WEB-SVAT predicted and observed surface radiometric temperature (T_R) during the 2001, 2002, 2003 and 2004 growing seasons.

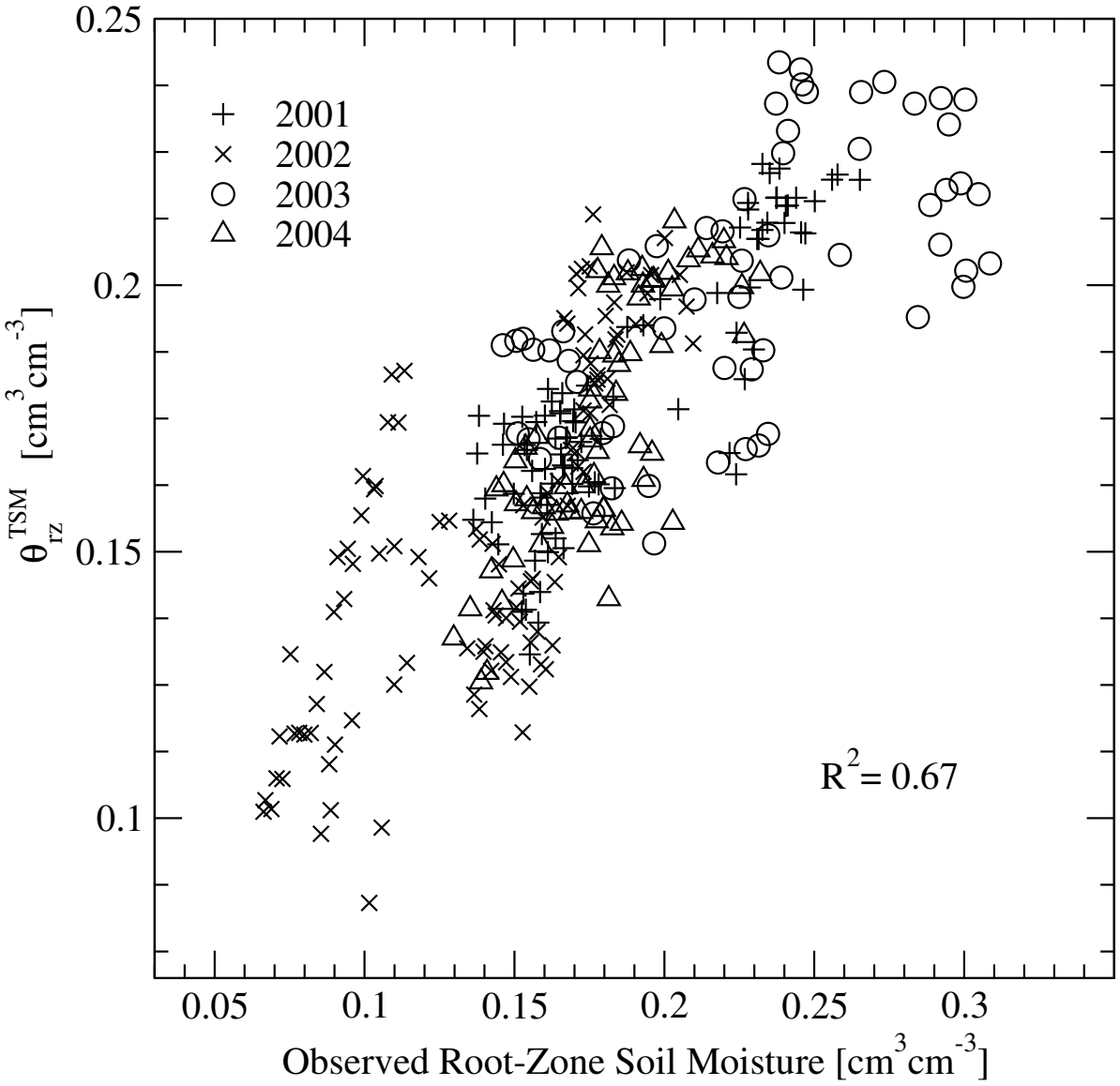

Fig. 5. Scatterplot of TSM root-zone soil stress proxy ($\theta_{\mathrm{rz}}^{\mathrm{TSM}}$) versus root-zone soil moisture observations during the 2001, 2002, 2003 and 2004 growing seasons.

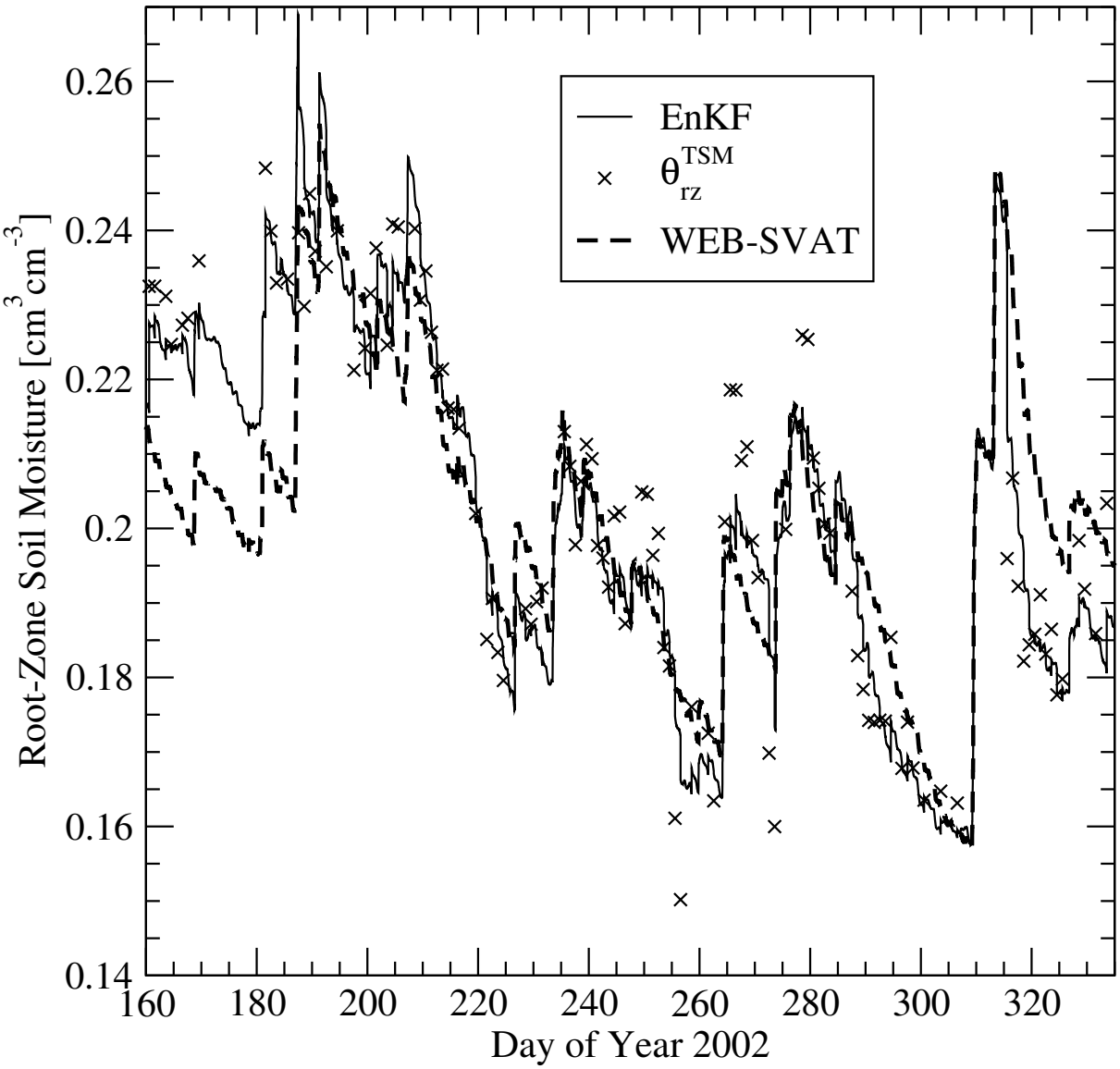

Fig. 6. Time series of WEB-SVAT predictions modified via the EnKF-based assimilation of the TSM/RS-SVAT root-zone soil moisture proxy ($\theta_{\rm rz}^{\rm TSM}$).

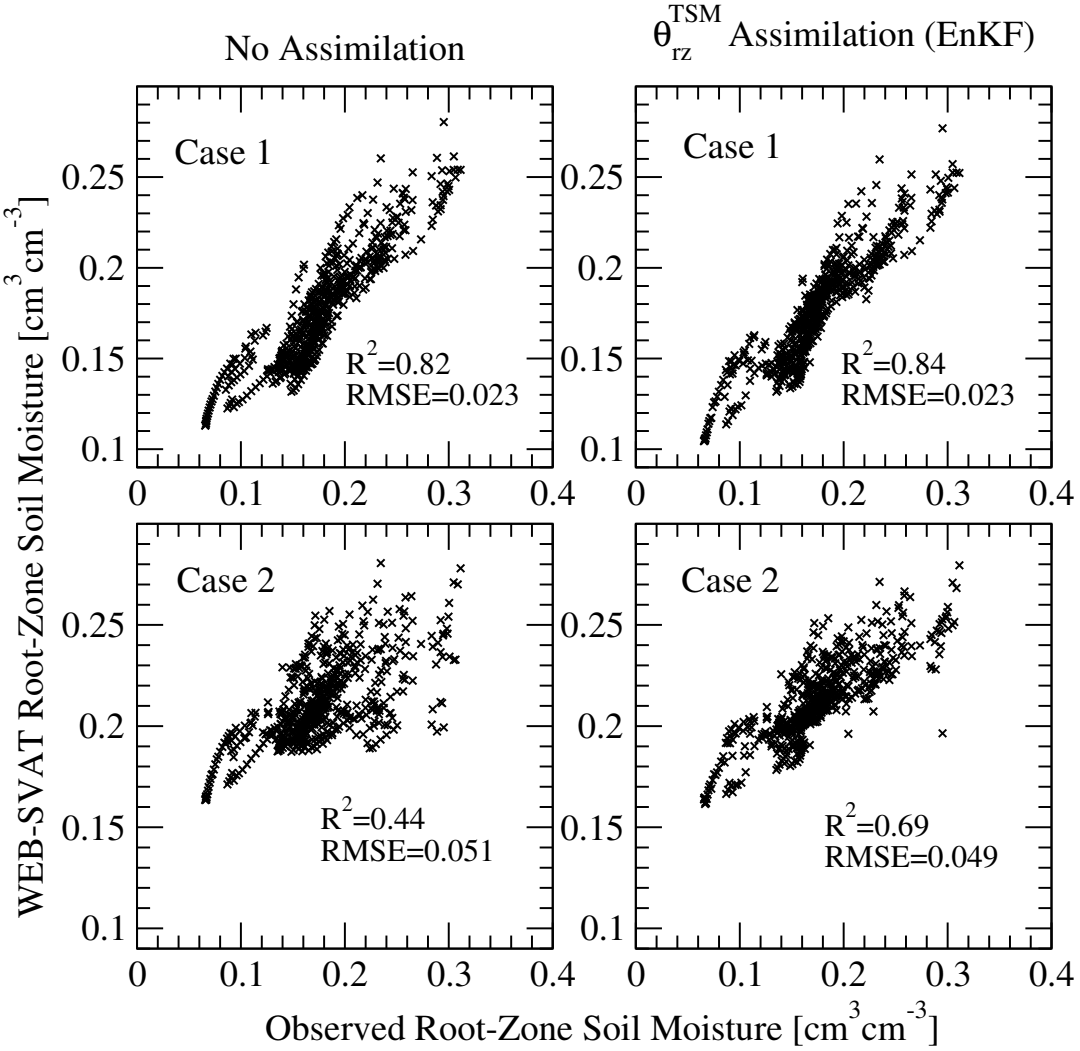

Fig. 7. Case 1 and 2 (see Table 1) scatterplots of WEB-SVAT and WEB-SVAT/EnKF θ_{rz}^{TSM} assimilation results for all days in the 2001, 2002, 2003 and 2004 growing seasons.

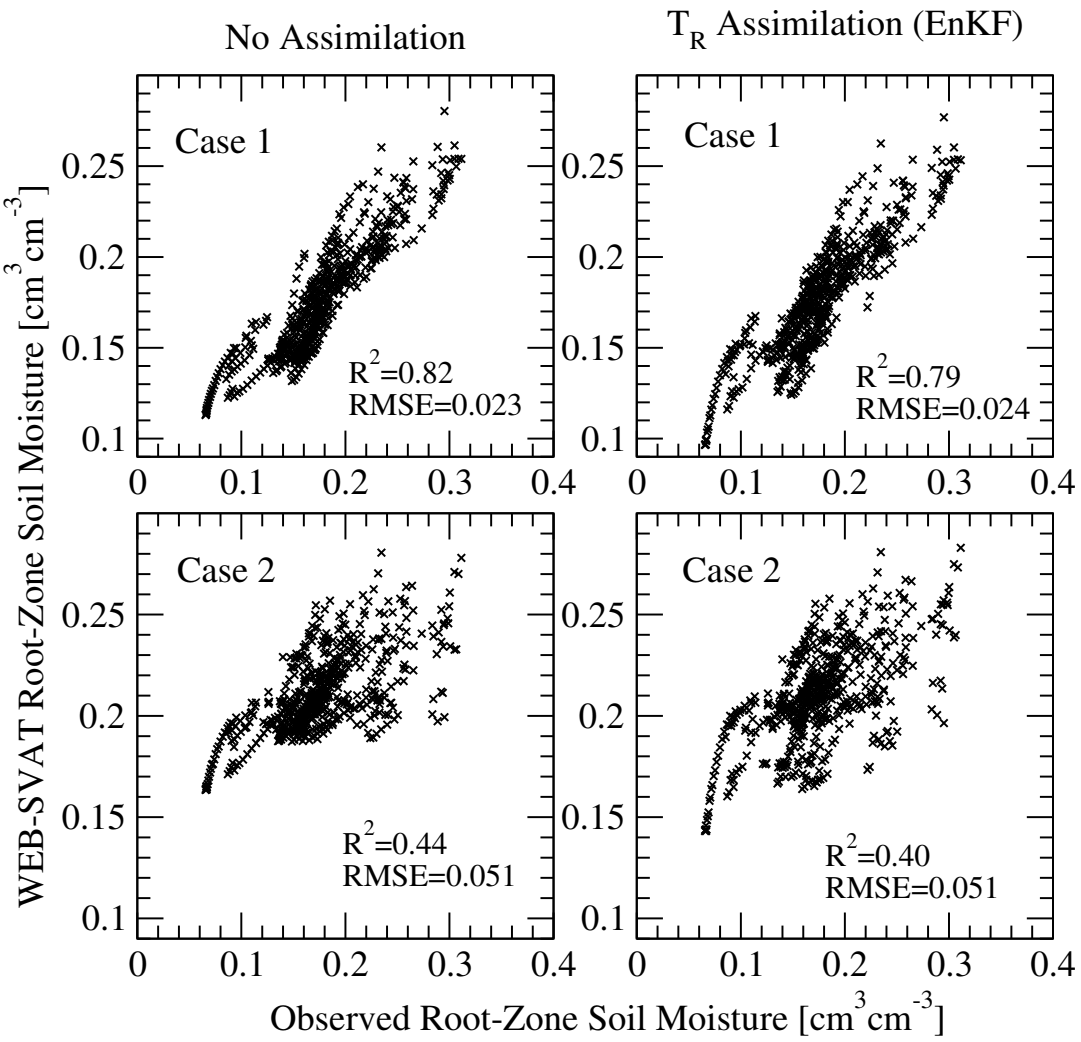

Fig. 8. Case 1 and 2 (see Table 1) scatterplots of WEB-SVAT and WEB-SVAT/EnKF T_R assimilation results for all days in the 2001, 2002, 2003 and 2004 growing seasons.

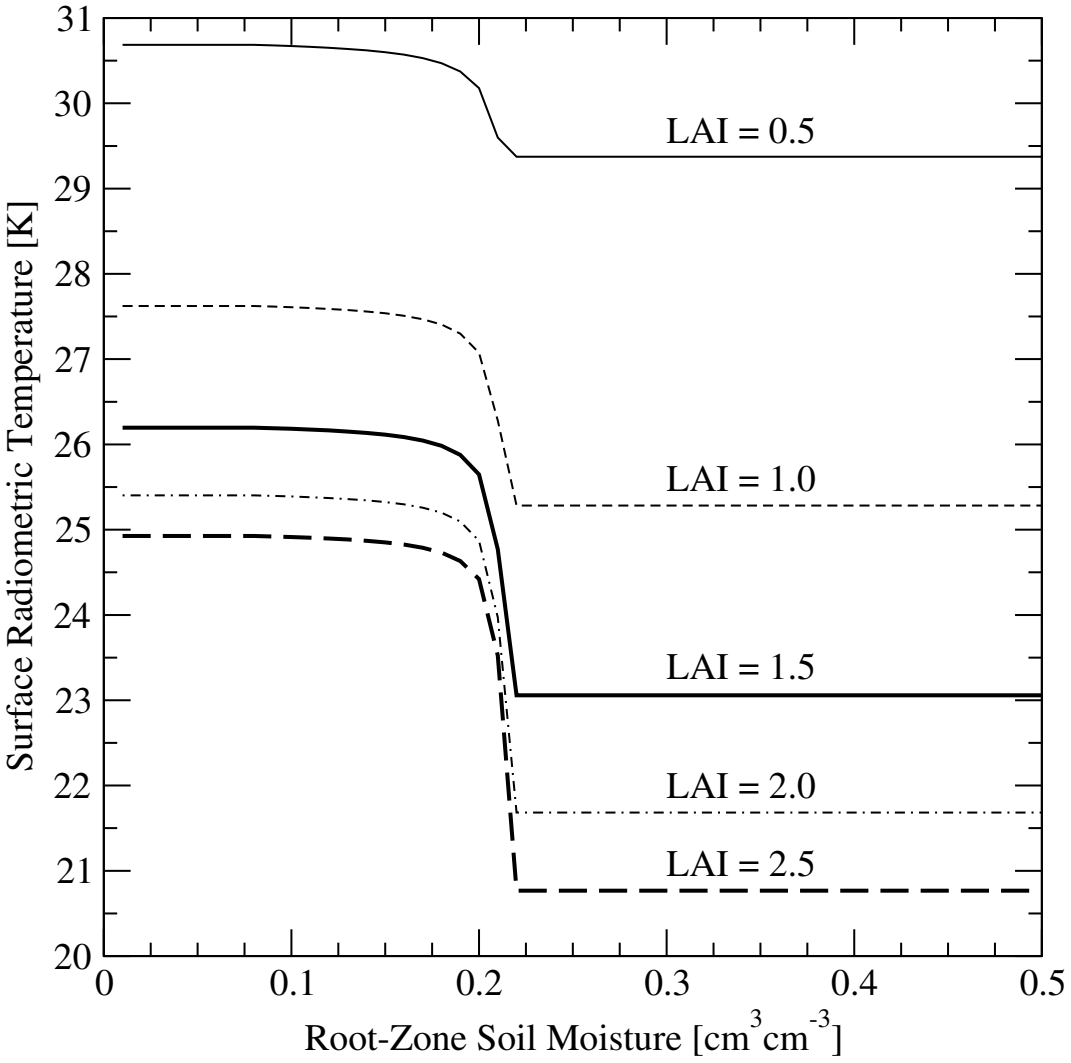

Fig. 9. For a range of leaf areas index (LAI) values, typical summer afternoon relationship predicted by the WEB-SVAT model between surface radiometric temperature (T_R) and root-zone soil moisture ($\theta_{\rm rz}$).

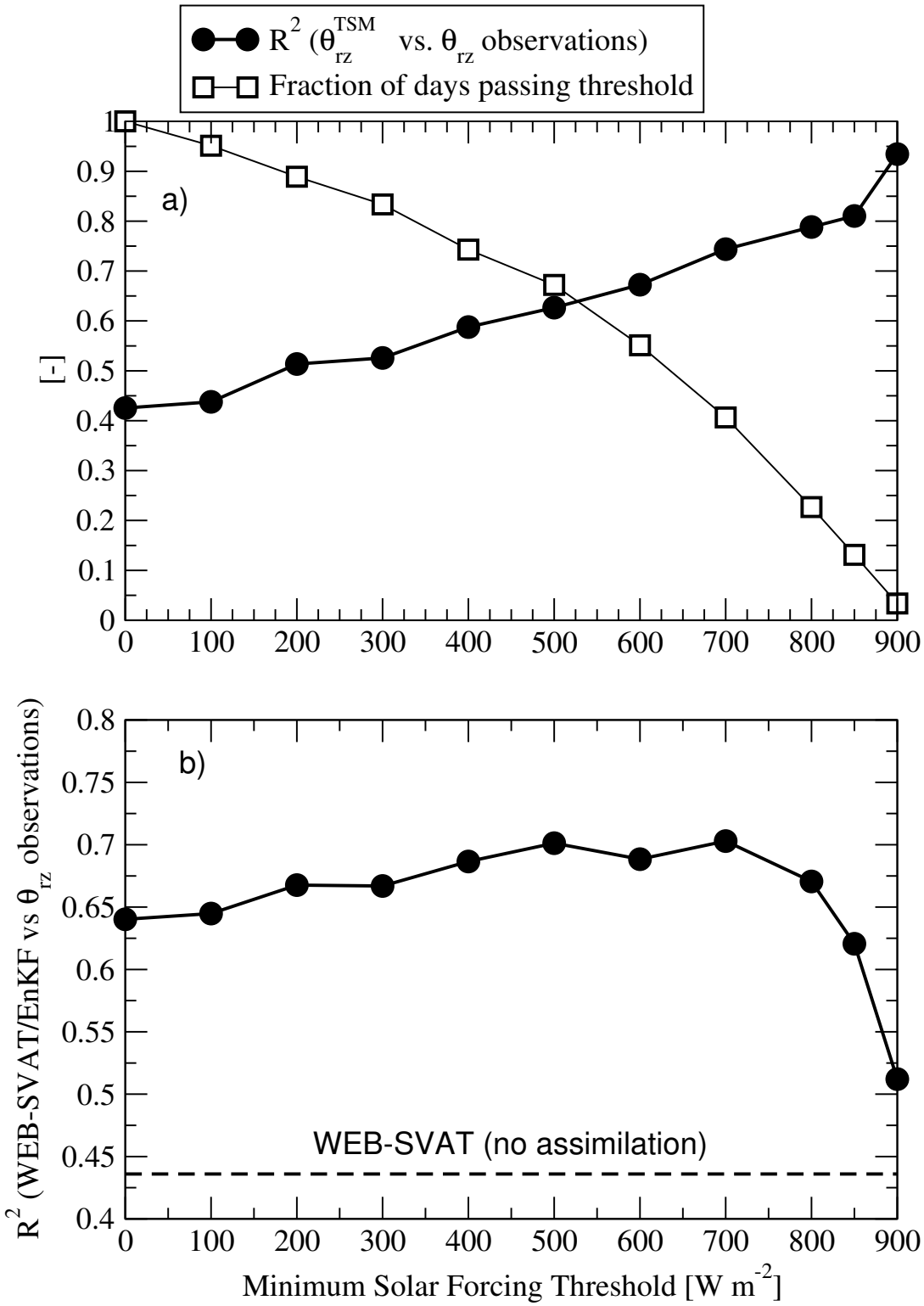

Fig. 10. a) Sensitivity of $\theta_{\mathrm{rz}}^{\mathrm{TSM}}$ root-zone proxy skill and observation frequency to variations in the minimum solar loading ($S_{\downarrow}$) threshold and b) the effect of this threshold on the accuracy of Case 2 WEB-SVAT/EnKF assimilation results (obtained through the assimilation of $\theta_{\mathrm{rz}}^{\mathrm{TSM}}$).

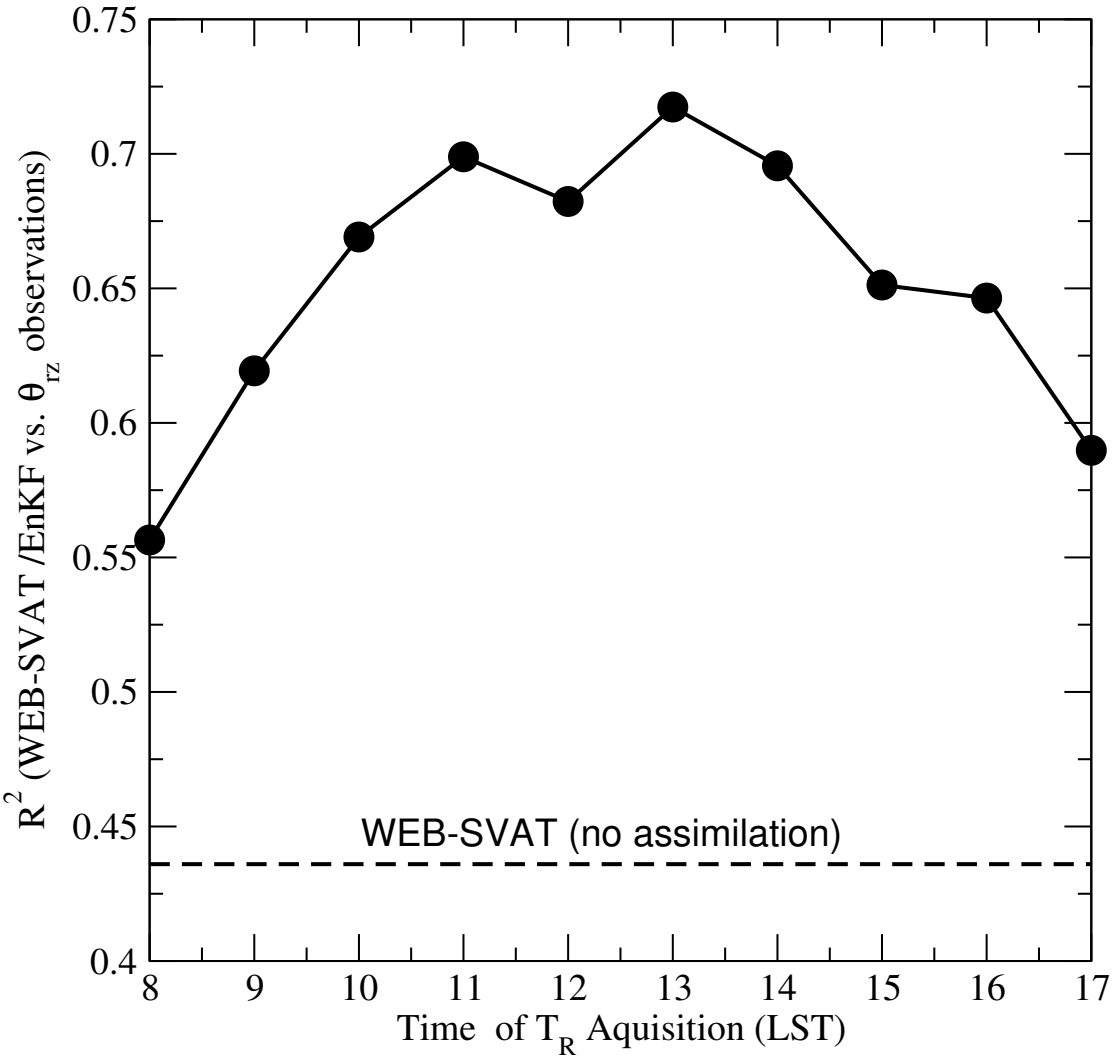

Fig. 11. The effect of T_R acquisition time on the accuracy of Case 2 WEB-SVAT/EnKF assimilation results (obtained through the assimilation of $\theta_{\mathrm{rz}}^{\mathrm{TSM}}$).

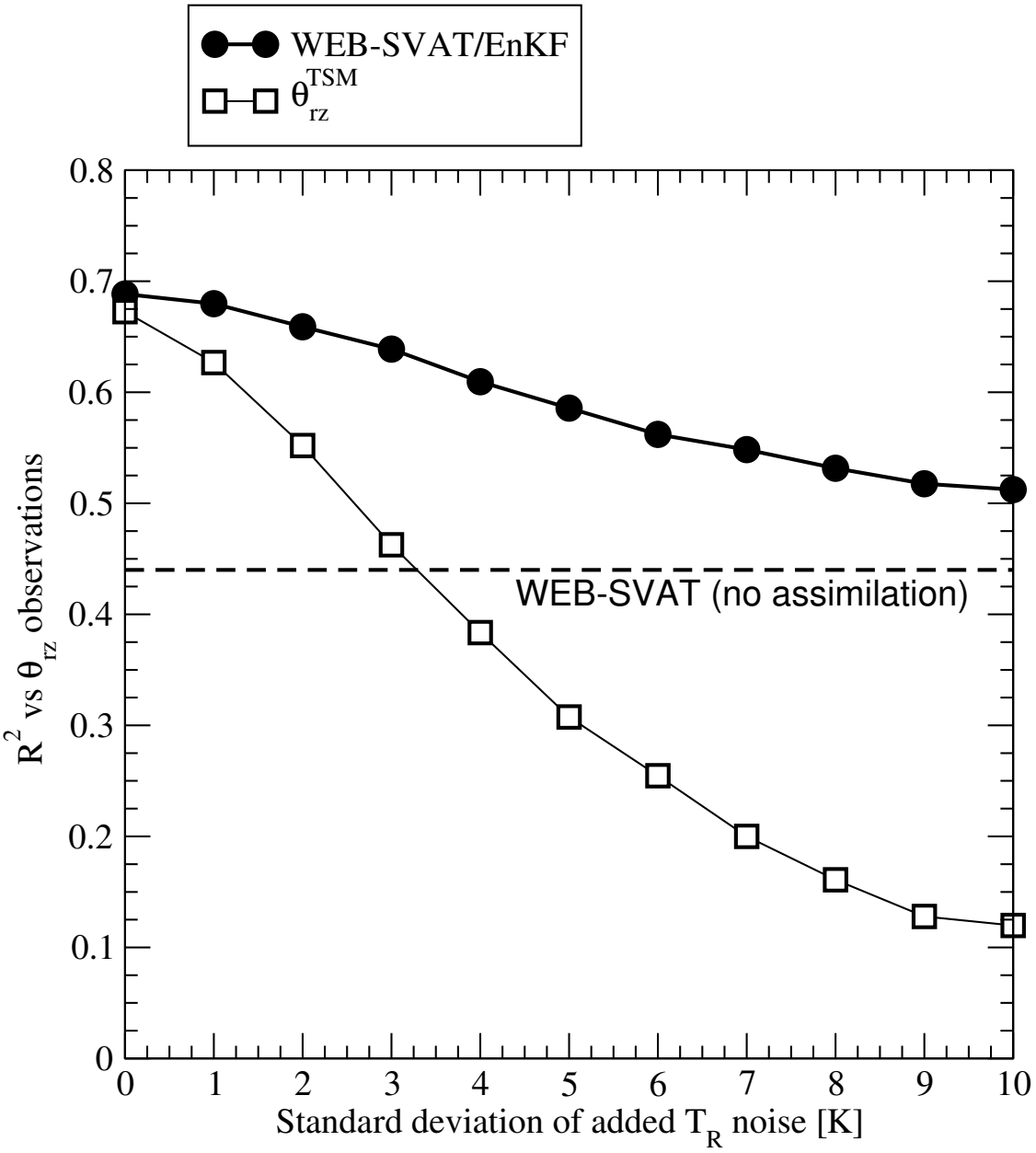

Fig. 12. Sensitivity of T_R measurement error to the accuracy of Case 2 WEB-SVAT/EnKF assimilation results (obtained through the assimilation of $\theta_{\rm rz}^{\rm TSM}$).